ARTICLE
PUBLISHED ONLINE: 5 FEBRUARY 2012 | DOI: 10.1038/NCHEMBIO.777
nature chemical biology

Computational redesign of a mononuclear zinc metalloenzyme for organophosphate hydrolysis

Sagar D Khare[1,10], Yakov Kipnis[1,10], Per Jr Greisen[2,10], Ryo Takeuchi[3], Yacov Ashani[4,5], Moshe Goldsmith[6], Yifan Song[1], Jasmine L Gallaher[1], Israel Silman[5], Haim Leader[7], Joel L Sussman[4], Barry L Stoddard[3], Dan S Tawfik[6] & David Baker[1,8,9]*

The ability to redesign enzymes to catalyze noncognate chemical transformations would have wide-ranging applications. We developed a computational method for repurposing the reactivity of metalloenzyme active site functional groups to catalyze new reactions. Using this method, we engineered a zinc-containing mouse adenosine deaminase to catalyze the hydrolysis of a model organophosphate with a catalytic efficiency (k_{cat}/K_m) of ~10^4 M^{-1} s^{-1} after directed evolution. In the high-resolution crystal structure of the enzyme, all but one of the designed residues adopt the designed conformation. The designed enzyme efficiently catalyzes the hydrolysis of the R_P isomer of a coumarinyl analog of the nerve agent cyclosarin, and it shows marked substrate selectivity for coumarinyl leaving groups. Computational redesign of native enzyme active sites complements directed evolution methods and offers a general approach for exploring their untapped catalytic potential for new reactivities.

The redeployment of catalytic machinery in naturally occurring enzyme active sites for noncognate reactions holds considerable promise as a method for obtaining new biocatalysts[1,2]. Alterations of substrate specificity and stereospecificity and the enhancement of preexisting promiscuous activities of enzymes have been accomplished by library-based directed evolution approaches[3]. However, introducing completely new catalytic activities remains a challenge with these approaches because a starting point with some activity is typically required for directed evolution. Though it is possible to introduce mechanistically related activities into enzymes, these approaches require homologs with the desired activity from which sequence or structural features can be borrowed[4–12].

Organophosphate pesticides and nerve agents, introduced into the environment in the 1950s, are highly toxic threat agents, and there is considerable interest in treating and mitigating their effects. Enzymes that rapidly hydrolyze organophosphate pesticides and the more toxic isomers of chiral nerve agents would be valuable as prophylactics and post-exposure treatments[13]. These enzymes may also serve as useful reagents for the bioremediation of contaminated sites. Naturally occurring enzymes with cognate or promiscuous organophosphate hydrolysis activity have been evolved to target the toxic isomers of some organophosphate compounds[14,15].

Computational enzyme design methods have been used to alter enzyme substrate specificity[16] and to design catalysts for reactions that are not known to be catalyzed by natural enzymes[17–19]. In *de novo* computational enzyme design, constellations of backbones that can support idealized active sites for the target reaction are identified in a set of protein scaffolds, and the sequence of the rest of the binding pocket is optimized for transition state affinity[20]. Because these efforts have been aimed at building active sites *de novo*, the reactivity of wild-type functional groups already present in the scaffold proteins is not considered in design.

Metal ions in enzyme active sites are highly reactive, and metal catalysis plays a key role in both enzymatic and abiological reactions. In particular, zinc ions serve as powerful catalysts in several hydrolase enzymes by providing an activated water molecule for nucleophilic attack, polarizing the scissile bond, stabilizing the developing negative charge on the transition state or a combination of the above[21].

Here we extend our *de novo* enzyme design methodology to exploit the reactivity of metal ions in existing enzyme active sites and use this strategy to design an organophosphate hydrolase starting from a functionally diverse set of mononuclear zinc-containing metalloenzyme scaffolds. On the basis of a native adenosine deaminase with $k_{cat}/K_m < 10^{-3}$ M^{-1} s^{-1} for the hydrolysis of an organophosphate substrate, we computationally engineered an organophosphate hydrolase with $k_{cat}/K_m \sim 10^4$ M^{-1} s^{-1} after activity maturation using directed evolution, representing a net increase in activity greater than 10^7-fold.

RESULTS

Computational design of an organophosphate hydrolase

We extracted a set of mononuclear zinc enzyme scaffolds with diverse wild-type functions and at least one open coordination site on the zinc atom from the Protein Data Bank (PDB). The requirement of at least one open zinc coordination site ensured that structural zinc sites were excluded from the scaffold set. The zinc coordination geometry in the scaffold set was either tetrahedral or trigonal bipyramidal.

The organophosphate hydrolysis reaction proceeds by an S_N2 mechanism such that the transition state geometry is trigonal bipyramidal around the phosphorus center[22]. To construct models of the reaction transition state, we used bond lengths and bond angles around the phosphorus reaction center from previously reported gas-phase quantum mechanical calculations[23] of the hydrolysis of paraoxon, with the modification that the lengths of the bonds being formed and broken around the phosphorus center were set to 1.6 Å

[1]Department of Biochemistry, University of Washington, Seattle, Washington, USA. [2]Department of Physics, Technical University of Denmark, Lyngby, Denmark. [3]Division of Basic Sciences, Fred Hutchinson Cancer Research Center, Seattle, Washington, USA. [4]Department of Structural Biology, Weizmann Institute of Science, Rehovot, Israel. [5]Department of Neurobiology, Weizmann Institute of Science, Rehovot, Israel. [6]Department of Biological Chemistry, Weizmann Institute of Science, Rehovot, Israel. [7]Department of Materials and Interfaces, Weizmann Institute of Science, Rehovot, Israel. [8]Howard Hughes Medical Institute, University of Washington, Seattle, Washington, USA. [9]Biomolecular Structure and Design Program, University of Washington, Seattle, Washington, USA. [10]These authors contributed equally to this work. *e-mail: dabaker@u.washington.edu

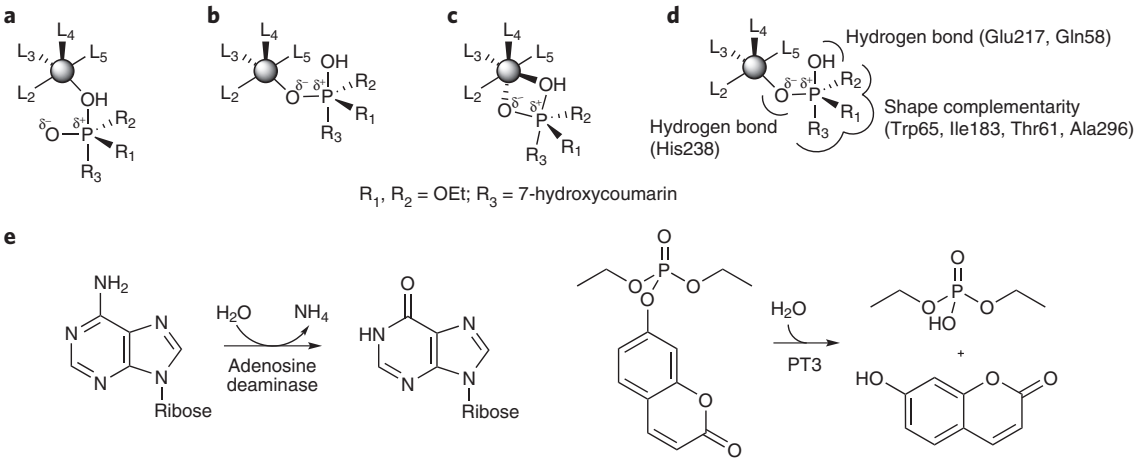

Figure 1 | Computational active site redesign. (**a**–**c**) Modeled transition geometries. The modeled organophosphate transition state was placed into a set of mononuclear zinc metalloenzyme active sites such that the zinc ion (gray spheres) acts as an activator of the nucleophilic hydroxyl moiety (**a**), stabilizes the developing negative charge on the phosphate moiety (**b**) or both (**c**). We generated similar alignments for tetrahedral zinc sites. (**d**) Additional hydrogen bonding interactions were derived from the original scaffold (for example, His238 in PT3) or introduced (for example, Gln58 in PT3) using the RosettaMatch algorithm. Shape complementary interactions to maximize transition state affinity were introduced using RosettaDesign. Residue numbers shown correspond to the PT3 design (described the results). (**e**) The wild-type adenosine deamination and the designed organophosphate hydrolysis reactions.

and 2.0 Å, respectively. We created a transition state ensemble by sampling the torsional degrees of freedom in the R1, R2 and R3 substituents (**Fig. 1**) of the transition state model while avoiding internal steric clashes. In hydrolytic metalloenzymes, metal ions act as activating agents for a hydroxyl ion nucleophile, as Lewis acids for stabilizing the charge on the transition state or as both. Therefore, we generated three corresponding alignments (**Fig. 1a**–**c**) of the transition state model with the wild-type metal center. Models of the transition states corresponding to two substrates, methyl paraoxon and diethyl 7-hydroxycoumarinyl phosphate (DECP), were placed into the active site of each member of the scaffold set according to each alignment. In each case, we used RosettaMatch[20] to search for additional hydrogen bonding interactions to the phosphoryl oxygen, the nucleophilic hydroxyl moiety and the leaving group oxygen. In cases where at least two of these three hydrogen-bonding interactions were found, we introduced shape complementary interactions to the transition state using RosettaDesign[24] (**Fig. 1d**). The coordination geometry around the metal ion during the design procedure was maintained by enforcing pseudocovalent restraints between the metal ion and the protein side chains coordinating the metal. We selected a set of 12 designed proteins (**Table 1**) for experimental characterization on the basis of the number of hydrogen-bond interactions to the transition state (>2), the transition state shape complementarity[25] (S_c >0.6) and the presence of a docking funnel[26], all of which ensured that alternative orientations of the transition state were higher in energy compared to the designed pose. One of these 12 proteins, a redesigned adenosine deaminase (scaffold PDB code 1A4L) that we called PT3, hydrolyzed the substrate DECP. Although organophosphate hydrolysis and adenosine deamination are both hydrolytic reactions (**Fig. 1e**), their transition state geometry, their leaving group character and the inherent reactivity of their substrate electrophilic centers are quite distinct.

Characterization and directed evolution of PT3

PT3 has eight mutations compared to the parent adenosine deaminase: the substitutions F65W, A183I, F61T, D19S, L62I, I299V and D296A provide shape complementarity to the transition state, and L58Q introduces a hydrogen bond to the nucleophile in the computational model (**Fig. 1d**). The zinc-coordinating residues His15, His17, His214 and Asp295 and the catalytic residues Glu217 and

Table 1 | List of designed proteins

Name (PDB ID)	Scaffold function	Expressed	Soluble	Active	Number of mutations
PT1 (2PLM)	Deaminase	Yes	No	No	10
PT2 (1N8K)	Alcohol dehydrogenase	Yes	No	No	7
PT3 (1A4L)	Adenosine deaminase	Yes	Yes	Yes	8
PT4 (1DQS)	Dehydroquinate synthase	Yes	No	No	10
PT5 (2QW5)	Sugar phosphate isomerase	Yes	Yes	No	11
PT6 (3H1W)	Mannose-6-phosphate isomerase	Yes	No	No	15
PT7 (3COS)	Alcohol dehydrogenase	Yes	No	No	5
PT8 (1H7N)	5-Aminolaevulinic acid dehydratase	Yes	Yes	No	8
PT9 (3HWP)	Diacetylphloroglucinol hydrolase	Yes	No	No	9
PT10 (1KQ3)	Glycerol dehydrogenase	Yes	Yes	No	11
PT11 (1ZSW)	Glyoxalase family protein	Yes	Yes	No	11
PT12 (2HBV)	2-Amino-3-carboxymuconate 6-semialdehyde decarboxylase	Yes	Yes	No	7

Designed proteins PT1–PT7 were made using methyl paraoxon and PT8–PT12 using DECP as the model substrate. The expression of the designed proteins in *E. coli* and their presence in the soluble fraction of the cell lysate was detected by SDS-PAGE analysis.

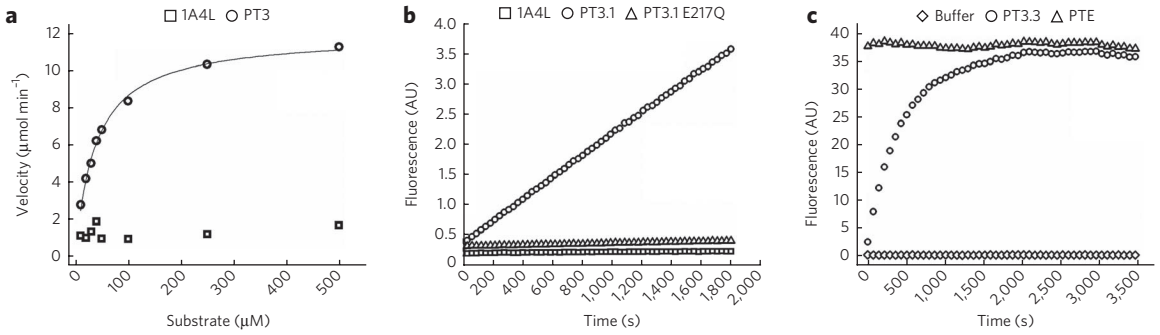

Figure 2 | Kinetic characterization of PT3 with DECP. (**a**) Michaelis-Menten analysis of the computationally designed PT3 variant and the wild-type adenosine deaminase (PDB code 1A4L) indicates a k_{cat}/K_m = 4 M^{-1} s^{-1} for PT3. Measurements were made at an enzyme concentration of 2.5 μM for both the designed and wild-type proteins. Measurements were made in triplicate, and a representative trace is shown. (**b**) The E217Q mutation in the evolved variant PT3.1 has organophosphate hydrolysis activity similar to that of the wild-type adenosine deaminase (PDB code 1A4L), pointing to the catalytic importance of Glu217. (**c**) Multiple turnovers (>140) are observed with PT3.3 with an enzyme concentration of 350 nM and DECP concentration of 50 μM. For estimating the fluorescence signal corresponding to complete hydrolysis of DECP, bacterial phosphotriesterase (PTE) at 10 μM was used to hydrolyze the substrate under identical conditions.

His238 were retained from the wild-type adenosine deaminase. Kinetic measurements showed that the activity of PT3 was approximately seven-fold higher than that of the buffer background, with protein and substrate concentrations of 2.5 μM and 50 μM, respectively. The products of the reaction were identical to those obtained with the wild-type bacterial phosphotriesterase enzyme (**Supplementary Results** and **Supplementary Fig. 1**), but the catalytic efficiency of PT3, measured by Michaelis-Menten analysis, was modest (k_{cat}/K_m = 4 M^{-1} s^{-1}; **Fig. 2a**). Wild-type adenosine deaminase showed no acceleration of organophosphate hydrolysis at <20 μM enzyme concentration, suggesting a k_{cat}/K_m below 10^{-3} M^{-1} s^{-1} (**Supplementary Fig. 2**). The E217Q variant of an activity-matured variant of PT3 (PT3.1, described below) showed an organophosphate hydrolysis activity with DECP identical to that of the wild-type deaminase (**Fig. 2b**), indicating that Glu217, a residue that is involved in proton shuttling in the deamination reaction[27], is also crucial for catalysis of the newly introduced organophosphate hydrolysis reaction. The wild-type mouse adenosine deaminase enzyme belongs to the amidohydrolase superfamily[28], and though some member enzymes of this superfamily catalyze organophosphate hydrolysis, they use dinuclear rather than mononuclear metal sites[29] and do not contain the substitutions introduced to obtain PT3.

To gain insight into the features missing from the computational design protocol, we performed directed evolution experiments aimed at enhancing organophosphate hydrolysis activity. We chose 12 positions, including 5 that were computationally designed but excluding the putative catalytic residues, surrounding the active site for saturation mutagenesis and screened variants at each position separately (described further in Methods). We found activity-enhancing mutations at 3 of the 12 positions. By recombining these substitutions, we obtained the variant PT3.1 ($PT3^{I62L\ V218\ V299E}$) with a ~40-fold higher catalytic efficiency than PT3 (**Table 2**). The I62L substitution reverted a computationally designed residue to its wild-type identity, V299E changed the identity of a computationally designed residue, and the largest single contributor to the enhancement, the V218F substitution (~20-fold increase), was at a position that was not considered during the computational design process.

We subsequently introduced random mutations in PT3.1 using error-prone PCR and found increased activity of the protein upon substitutions at three positions (Ser57, Pro59 and Glu186). Saturation mutagenesis at these positions led to the identification of the variant PT3.2 ($PT3.1^{S57D\ P59K\ E186D}$) with an approximately ten-fold higher catalytic efficiency compared to PT3.1 (**Table 2**). Finally, modeling the interaction of the transition state with the crystal structure of apoPT3.1 (described below) suggested that Gln58 was suboptimal for activity. We performed saturation mutagenesis at this position and identified the variant PT3.3 ($PT3.2^{Q58V}$) with an approximately ten-fold higher catalytic efficiency compared to PT3.2. The variant PT3.3 had a catalytic efficiency (k_{cat}/K_m = 9,750 $M^{-1}s^{-1}$) approximately 2,500-fold higher than the initial PT3 variant (**Table 2**). Product inhibition leading to low total turnover numbers can be an issue for metallohydrolases, but PT3 proceeded through multiple turnovers; at an enzyme concentration of 350 nM, PT3.3 completely hydrolyzed 50 μM DECP, indicating >140 catalytic turnovers per enzyme molecule (**Fig. 2c**).

As the designed organophosphate hydrolysis activity increased during directed evolution, there was a concomitant decrease in the deamination activity. The variant PT3 had an adenosine deamination activity that was ~50,000-fold less than that of the deaminase, whereas in the evolved variant PT3.1 deamination activity was undetectable (**Supplementary Fig. 3**). To uncover the minimal set of mutations required to endow the deaminase with the designed organophosphate hydrolysis activity, we reverted each position in PT3.3 to its wild-type deaminase identity, one at a time. In parallel, starting from the deaminase, we generated a library of variants (WTtoPT3 set) in which the substitutions corresponding to PT3 were present in random combinations. We screened these libraries as cell lysates for organophosphate hydrolysis activity with DECP and sequenced select variants. In both cases, we found that four substitutions in the deaminase (D19S, F61T, A183I and D296A) were required to be simultaneously present for organophosphate hydrolysis activity to emerge. All variants with detectable DECP hydrolysis activity from the WTtoPT3 set (**Supplementary Table 1**) had these four substitutions simultaneously.

There was striking spatial clustering (**Fig. 3** and **Supplementary Table 2**) of the mutations that enhanced PT3 activity—primarily by

Table 2 | Kinetic parameters for DECP hydrolysis

Variant	k_{cat} (× 10^{-3} s^{-1})	K_m (μM)	k_{cat}/K_m (M^{-1} s^{-1})
1A4L (wild type)	5 × 10^{-5} ± 1 × 10^{-5}	>500	<10^{-3}
PT3	0.2 ± 0.1	43 ± 2	4 ± 2
PT3.1	4 ± 1	26 ± 1	154 ± 39
PT3.2	47 ± 5	49 ± 3	959 ± 118
PT3.3	351 ± 26	36 ± 5	9,750 ± 1,534

Errors were estimated using s.d. in k_{cat} and K_m from triplicate measurements.

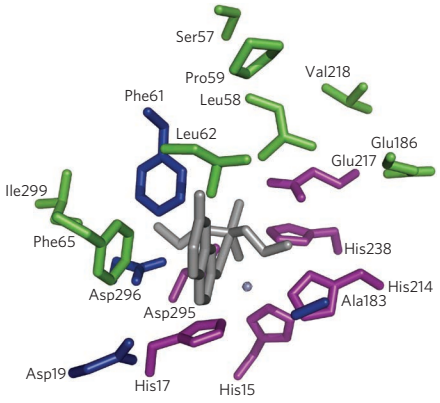

Figure 3 | Spatial clustering of wild-type and activity-enhancing residues. Residues in which computationally designed simultaneous substitutions were essential for the emergence of organophosphate hydrolysis activity are highlighted in blue. Deaminase residues retained in the most active variant of PT3 (purple), and positions in which activity-enhancing mutations occur during directed evolution (green) form two separate spatial clusters. Residue side chain identities are from the deaminase crystal structure (PDB code 1A4L), and the transition state model is shown in gray sticks.

increasing k_{cat} (**Table 2**)—suggesting that these residues fine-tuned the alignment of the substrate in the active site, increased the pK_a of Glu217 by increasing hydrophobicity around this putative catalytic base (for example, substitutions V218F and Q58V) or both (**Fig. 1d**). This residue has an elevated pK_a in the wild-type deaminase[27], and the calculated pK_a of Glu217 in the crystal structure of the evolved variant PT3.1 (described below) was higher by 1.6 ΔpH units than in the model of PT3 (**Supplementary Table 3**). These results suggest that the increase in activity observed during the course of directed evolution was related to an increase in the basicity of Glu217.

Crystal structure of apoPT3.1

We determined the crystal structure of the variant PT3.1 ($PT^{3I62L\ V218F\ V299E}$) to 2.35-Å resolution. In the crystal structure, the TIM–barrel fold of the deaminase was maintained, and the overall backbone conformation was quite similar (backbone r.m.s. deviation = 0.65 Å) to that of the PT3 design model (**Fig. 4a**). The zinc binding site and other elements of the wild-type catalytic machinery that were retained in the designed protein (for example, residues His238, Glu217 and Asp295) maintained their wild-type conformations. We observed clear density indicating a zinc-bound water molecule and found that the trigonal bipyramidal zinc coordination geometry from the deaminase was maintained in PT3.1. All computationally designed residues of PT3.1 except Gln58 adopted rotamers predicted by the computational model (**Fig. 4b**,**c**).

Two loops that border the active site and connect sequential β–α elements within the core TIM barrel fold (β4–α4 and β5–α5, respectively) each showed backbone conformational differences compared to the deaminase structure and to their predicted conformation in the original PT3 computational design model (**Fig. 4a**). Loop I, composed of residues 183–194, was displaced by approximately 2 Å away from the mouth of the β-barrel. This conformational difference involved only small alterations of backbone dihedral angles, such that the loop was displaced with little overall change in its peptide conformation and most likely results from electrostatic repulsion between the Asp185 and Gln58 side chains.

Loop II, composed of residues 217–221, contains the V218F mutation that provided a substantial contribution (20-fold) to rate enhancement for the PT3.1 construct. The side chain for Phe218 was well ordered and was in close proximity to the side chains of Glu217 and Gln58. In contrast, the surrounding residues of loop II showed density consistent with two distinct conformations (one of which resembled the structure of the original deaminase). The side chain of Gln58 was found in an alternate rotameric conformation relative to the original computational design, suggesting that the addition of V218F during directed evolution led to the inversion of the Gln58 rotamer (**Fig. 4d**).

Substrate selectivity and stereoselectivity of PT3

Both the computational design and directed evolution of PT3 were performed with the nonchiral substrate DECP. To investigate the substrate specificity of the designed organophosphate hydrolysis activity, we used several substrates, each with different substituents on the phosphate moiety (described in Methods). To our surprise, we found that PT3 efficiently hydrolyzed substrates with a coumarinyl leaving group (DECP, 7-*O*-diethylphosphoryl-3-cyano-7-hydroxycoumarin (DEPCyC) and methylphosphonic acid 3-cyano-4-methyl-2-oxo-2H-coumarin-7-yl ester cyclohexyl ester (CMP-coumarin); **Fig. 5** and **Supplementary Fig. 4**) but did not hydrolyze substrates that have substituted phenyl-ring leaving groups (for example, paraoxon, 4-nitrophenyl diethyl phosphate), despite their similar intrinsic reactivity. We found that both paraoxon and 4-nitrophenol inhibited the reaction of PT3 with DECP (K_i ~ 250 μM and ~150 μM, respectively; **Supplementary Fig. 5**), but there was no evidence of product inhibition with DECP (**Fig. 2c**). Docking calculations indicated that the smaller size of the

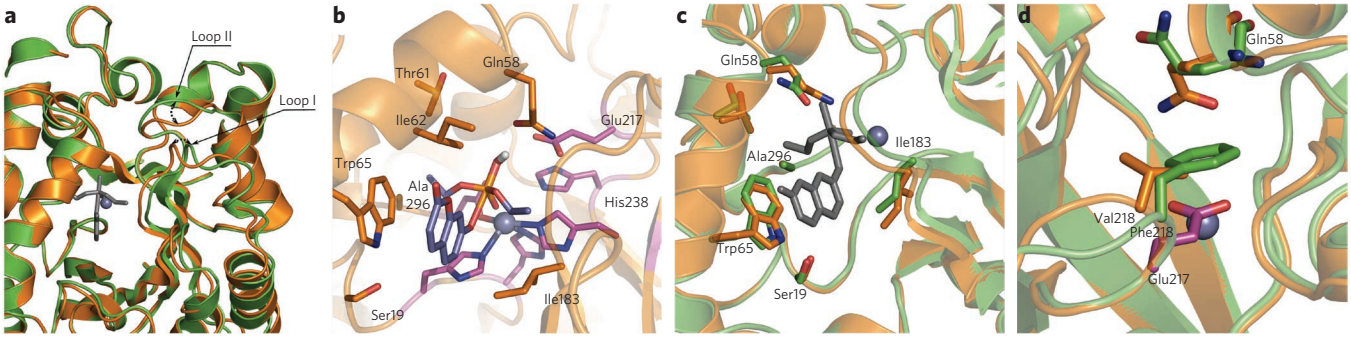

Figure 4 | Design model and crystal structure of apoPT3.1. (**a**) Superposition of the PT3.1 design model (gold) and the crystal structure (green) shows that although the overall backbone similarity is high (backbone r.m.s. deviation = 0.65 A), there are small shifts in two active site–proximal loops. (**b**) The PT3 design model showing alignment of the transition state in the redesigned enzyme. (**c**,**d**) Side chains of designed residues Ser19, Trp65, Ile183 and Ala296 observed in the crystal structure (green) adopt rotamers predicted in the designed model (gold, **c**), whereas the side chain of residue Gln58 adopts a different rotamer in the crystal structure (green) compared to the designed rotamer (gold, **d**), which corresponds to a change in its χ_2 dihedral angle.

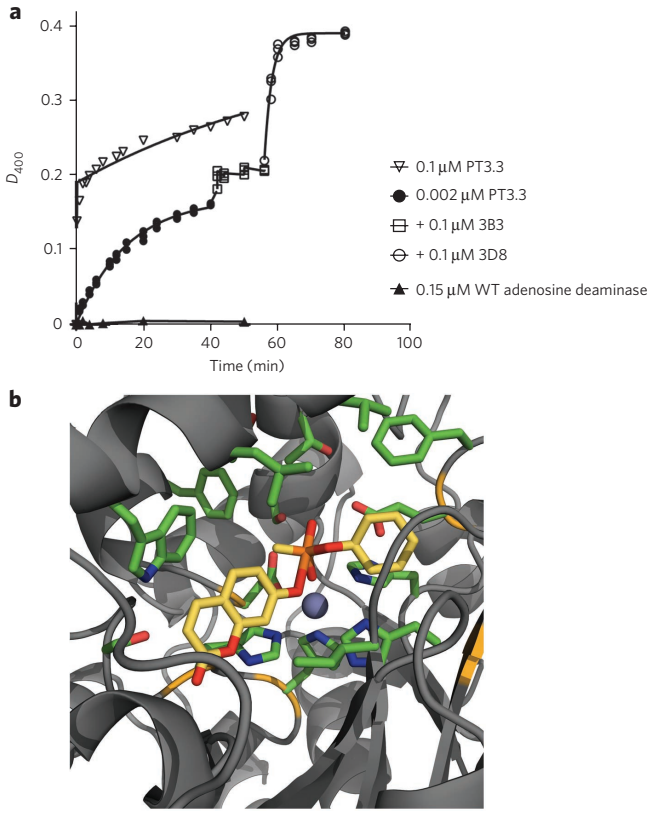

Figure 5 | PT3 variants stereo-selectively catalyze the hydrolysis of a cyclosarin analog. (**a**) Release of the coumarin leaving group from ~10 μM racemic mixture of CMP-coumarin with the indicated enzyme was monitored by measuring absorbance at 400 nm (D_{400}). After incubating 0.002 μM PT3 with CMP-coumarin so that D_{400} reached a plateau, the variant 3B3 of the recombinant mammalian-like serum paraoxonase that selectively hydrolyzes the R_P form of CMP-coumarin was added. When D_{400} in the presence of 3B3 reached the ~0.2 D_{400} plateau, the reaction mixture was spiked with the 3D8 variant of the paraoxonase, which hydrolyzes both the R_P and S_P isomers[14,37] and allows the detection of the presence of the intact S_P isomer. The resulting increase in D_{400} to ~0.4 demonstrates the stereopreference of PT3.3 for the R_P isomer. The observed burst phase (resulting in D_{400} ~ 0.2) and biphasic behavior with a PT3 concentration of 0.1 μM suggests that the S_P isomer is hydrolyzed by PT3, albeit at a much slower rate than the R_P isomer. All data were collected in triplicate, and a representative trace is shown. (**b**) Model of the CMP-coumarin transition state docked into the PT3 crystal structure. The cyclohexyl moiety occupies the open pocket of PT3, consistent with the observed preference for the R_P isomer. WT, wild-type.

nitrophenyl group allowed a greater variety of alternative binding modes for paraoxon in the active site pocket, greatly reducing the fraction of bound configurations productively aligned with the catalytic machinery (**Supplementary Fig. 6**). These alternative binding modes, presumably driven by the binding of the phenyl ring, also sterically precluded the simultaneous binding of DECP and may thereby inhibit the reaction of PT3 with DECP.

The variants PT3.1–PT3.3 efficiently hydrolyzed the coumarinyl analog of the racemic nerve agent surrogate of cyclosarin, CMP-coumarin. PT3.3 had a marked stereopreference for the R_P isomer of CMP-coumarin, whereas the wild-type deaminase showed no detectable activity with either isomer of CMP-coumarin at the same concentration (**Fig. 5a**). Despite the pronounced stereopreference of PT3.3 for the R_P isomer, we also observed slow hydrolysis of the S_P isomer (an R_P/S_P kinetic ratio >150). These results are consistent with the modeled alignment of CMP-coumarin in the PT3.3 active site (**Fig. 5b**). For the actual nerve agent cyclosarin, the more toxic S_P isomer was not hydrolyzed by any PT3 variant (data not shown). However, given that the design model is consistent with the observed stereopreference and in view of the slow but detectable hydrolysis of the S_P isomer of the cyclosarin surrogate, it should be possible to use the same approach to explicitly design catalysts to hydrolyze the toxic S_P isomer of nerve agents.

DISCUSSION

The high reactivity of metalloenzymes and the large diversity of reactions they carry out make them attractive starting points for the introduction of new activities. We chose zinc-containing enzymes as templates for computational design of organophosphate hydrolysis activity because zinc performs diverse mechanistic roles in enzymes, is redox stable and is used as a Lewis acid–type catalyst in many natural hydrolases[21], including the dinuclear bacterial organophosphate hydrolases. Computational design of mononuclear zinc-containing active sites successfully identified a set of mutations in an adenosine deaminase that endowed it with the target organophosphate hydrolysis activity. We considered only the geometric compatibility of the transition state with the active site structure during design and did not use *a priori* knowledge about the wild-type activity in scaffold identification. We found that four simultaneous mutations were required for the emergence of organophosphate hydrolysis activity in the deaminase (**Fig. 3**), and thus identification of the computationally designed variant by library screening would most likely have required generating and screening a library of an exceedingly large size. Having obtained the initial low-activity lead from computational design, we enhanced its activity by approximately 2,500-fold using directed evolution, demonstrating the power of computational design followed by directed evolution for enzyme redesign.

In contrast with the dinuclear zinc-containing bacterial phosphotriesterases, PT3 is a mononuclear zinc enzyme. In the dinuclear phosphotriesterases, one zinc ion polarizes the scissile P-O bond, and the μ-hydroxyl moiety bridging the zinc ions acts as the nucleophile[22]. Because we observed only one free zinc coordination site in the crystal structure of apoPT3, the zinc ion could act either to polarize the P-O bond (**Fig. 1b**) or to activate the nucleophile (**Fig. 1a**). In the wild-type adenosine deaminase, the zinc ion activates the hydroxyl nucleophile[27], whereas in the design model it polarizes the P-O bond along with the side chain of His238, and Glu217 activates the nucleophile by functioning as a general base. The increased hydrophobicity around the Glu217 side chain during directed evolution, the stereopreference for the R_P isomer of CMP-coumarin (**Fig. 5**) and the lack of activity of the E217Q variant (**Fig. 2b**) of PT3 are consistent with the placement of the transition state in the design model (**Fig. 1b**) and the role of Glu217 as a general base. Glu217 shuttles protons in the wild-type deaminase[27], and metal ion polarization of the P-O bond has been proposed for the organophosphate hydrolase diisopropyl fluorophosphatase, which has a single calcium ion in the active site[30]. However, in the absence of a substrate- or transition state analog–bound structure of PT3, the possibility that the zinc ion and the residues His238 and Asp295 activate the nucleophile while the protonated form of Glu217 helps polarize the P-O bond (**Fig. 1a**) cannot be definitively ruled out.

Shortcomings of the computational enzyme design protocol[31] and avenues for further improvement were highlighted by analyses of the sequence changes accrued during directed evolution and by comparisons of the crystal structure of the evolved variant PT3.1 to the design model. Most improvements in catalytic efficiency during directed evolution were increases in k_{cat}, and the largest single increase arose from the substitution V218F (variant PT3.1). The side chain at position 218 is not expected to directly contact the transition state, but V218F increases the hydrophobic bulk around the catalytically

critical Glu217 side chain, which probably modulates its pK_a and reactivity. Furthermore, the crystal structure of PT3.1 shows that the backbone structure of the loop composed of residues 217–221 needs to change conformation to accommodate the bulkier phenylalanine side chain introduced by the V218F mutation. As the design procedure is carried out on a fixed (wild-type) backbone, the V218F substitution would cause steric clashes in the design model. Allowing backbone flexibility in the design procedure and incorporating pK_a effects using a more accurate electrostatic interaction model are important areas for current methods development.

The computational active site redesign method described here is general and can be readily applied to the generation of biocatalysts for other reactions of interest. The method complements current library-based directed evolution approaches for enzyme engineering. Optimization of the computationally generated leads with directed evolution approaches has the potential to both substantially enhance the desired activities and provide valuable feedback for incorporating key missing elements in the computational design methodology. The vast diversity of highly reactive catalytic microenvironments in structurally well-characterized natural enzymes represents a rich resource of reactivity for obtaining new biocatalysts using computational enzyme redesign.

METHODS

Protein expression, purification and kinetic measurements. Designed proteins were expressed in *Escherichia coli* BL21 (DE3) using the pET29b plasmid (Novagene) and were purified over a nickel–nitriloacetic acid (Ni-NTA) affinity column. Protein purity and integrity were verified by SDS-PAGE. For PT3 variants, protein concentration was estimated spectrophotometrically using a calculated molar extinction coefficient of 50,000 M^{-1} cm^{-1}. Reaction progress was monitored by following the increase in fluorescence of the 7-hydroxycoumarin product (excitation (365 nm)/emission (445 nm)) in 10 mM HEPES, 150 mM NaCl buffer (pH 7.5) at a protein concentration of 2.5 μM. Initial rates of DECP (Sigma) decomposition were determined at 10–500 μM of substrate and were fit to the Michaelis-Menten equation $v_0 = k_{cat}\,[E]_0\,[S]_0 / (K_m + [S]_0)$ to obtain k_{cat} and K_m. Results of at least three independent measurements were used to calculate reported kinetic parameters and estimate errors.

Library construction and screening. Desired positions in the gene were changed or diversified using either the Kunkel method[32] or QuickChange mutagenesis (Stratagene) using mutagenic oligonucleotides (IDT). Error-prone PCR was performed using GeneMorphII kit (Stratagene) according to the manufacturer's instructions. Genes were cloned into the pET29b expression vector, and constructed libraries were transformed into the *E. coli* BL21 (DE3) strain. Depending on the estimated complexity of the library, 100–800 variants were assayed in screening experiments. Single colonies were grown in 96–deep-well plates. After cell lysis, activity of the protein variants was assayed in clarified lysate with 50 μM DECP. Improved variants were sequenced, and mutations responsible for improvements were recombined, before proceeding to the next round.

Crystal structure determination. After PT3.1 expression, purification and His_6 tag cleavage (**Supplementary Methods**), the purified protein was concentrated to 0.2 mM in 20 mM HEPES-NaOH, 100 mM sodium glutamate (pH 7.5) and 0.1 mM zinc acetate and was mixed with a 2.5-fold excess of sodium orthovanadate and 7-hydroxycoumarin. The crystal was obtained in 0.1 M Tris-HCl (pH 7.0), 0.2 M calcium acetate and 20% (w/v) PEG 3000 and was frozen by looping and submersion into liquid nitrogen. The crystal diffracted up to approximately 2.35-Å resolution at the ALS beam line 5.0.1. The data set was processed using the HKL-2000 package[33], and a murine adenosine deaminase (D295E; PDB code 1FKW) was used as a search model for molecular replacement. A single copy of the search model was found by PHASER[34] and was refined using REFMAC5[35]. The final model was deposited in the PDB with accession code 3T1G. Statistics for the crystallographic data are shown in **Supplementary Table 4**. The anomalous difference Fourier map was used to conclude that PT3.1 contains a heavy metal atom in its active site (**Supplementary Fig. 7**).

Determination of substrate specificity. Substrate specificity of the PT3 variants was tested using 2,4-dinitrophenyldiethylphosphate, 4-diethylphosphatebenzaldehyde, 4-nitrophenyldiethylphosphate (paraoxon; Sigma), 4-nitrophenyldimethylphosphate (methylparaoxon; Sigma) and DEPCyC. The synthesis and characterization of DEPCyC, 2,4-dintrophenyldiethylphosphate and 4-diethyl phosphate benzaldehyde were performed as described previously[36] (structure and purity verified by ^{1}H NMR). Next, 0.5–1 mM of the organophosphate compound was incubated with 5–10 μM of protein for 30 min. Change in absorbance or fluorescence at appropriate wavelength was recorded. The inhibitory effect of 2,4-dinitrophenyldiethylphosphate, paraoxon or 4-nitrophenol (Sigma) on the decomposition of DECP was studied by recording the rate of hydrolysis of 50 μM DECP in the presence of 0.025–1 mM inhibitor. The half-maximal inhibitory concentration (IC_{50}) was calculated by fitting into the equation $V_i = V_0 / (1 + I_i / IC_{50})$, where V_0 is the rate of the reaction in the absence of inhibitor and V_i is the reaction rate at inhibitor concentration I_i.

Determination of stereopreference with CMP-coumarin. The stereopreference of the PT3 variants when reacting with chiral organophosphates was determined with racemic CMP-coumarin as a substrate using the previously reported stereopreference of two engineered mammalian serum paraoxonase variants, rePON1s 3B3 and 3D8 (refs. 14,37). The synthesis and determination of exact concentration of the CMP-coumarin stock solution was performed as described previously[37] (structure and purity verified by thin layer chromatography and ^{1}H NMR). Approximately 10 μM of racemic CMP-coumarin was incubated with 2–100 nM PT3 variant in 50 mM Tris-100 mM NaCl, pH 8.0 at 25 °C, and the release of the leaving group 3-cyano-7-hydroxy-4-methylcoumarin was monitored by measuring absorbance at 400 nm. To identify the configuration of the nonhydrolyzed isomer in solution after the reaction approached an end point, the mixture was spiked first with 0.1 μM 3B3 and 1 mM $CaCl_2$, inducing the exclusive hydrolysis of residual R_P isomer. Additional spiking with 0.1 μM 3D8 revealed the presence and concentration of the intact S_P isomer. Detoxification of cyclosarin was carried out by monitoring the loss of anti–acetylcholine esterase potency as described previously[14].

Accession codes. PDB: the structure of the designed organophosphate hydrolase is deposited under accession code 3T1G. The previously published structures of the wild-type adenosine deaminase and murine adenosine deaminase are deposited under accession codes 1A4L and 1FKW, respectively.

Received 14 September 2011; accepted 25 October 2011; published online 5 February 2012

References

1. Toscano, M.D., Woycechowsky, K.J. & Hilvert, D. Minimalist active-site redesign: teaching old enzymes new tricks. *Angew. Chem. Int. Ed. Engl.* **46**, 3212–3236 (2007).
2. Gerlt, J.A. & Babbitt, P.C. Enzyme (re)design: lessons from natural evolution and computation. *Curr. Opin. Chem. Biol.* **13**, 10–18 (2009).
3. Khersonsky, O. & Tawfik, D.S. Enzyme promiscuity: a mechanistic and evolutionary perspective. *Annu. Rev. Biochem.* **79**, 471–505 (2010).
4. Yin, de L.T. *et al.* Switching catalysis from hydrolysis to perhydrolysis in *Pseudomonas fluorescens* esterase. *Biochemistry* **49**, 1931–1942 (2010).
5. Terao, Y., Miyamoto, K. & Ohta, H. Introduction of single mutation changes arylmalonate decarboxylase to racemase. *Chem. Commun. (Camb.)* **2006**, 3600–3602 (2006).
6. Schmidt, D.M.Z. *et al.* Evolutionary potential of $(\beta/\alpha)_8$-barrels: functional promiscuity produced by single substitutions in the enolase superfamily. *Biochemistry* **42**, 8387–8393 (2003).
7. Leopoldseder, S., Claren, J., Jurgens, C. & Sterner, R. Interconverting the catalytic activities of $(\beta\alpha)_8$-barrel enzymes from different metabolic pathways: Sequence requirements and molecular analysis. *J. Mol. Biol.* **337**, 871–879 (2004).
8. Williams, S.D. & David, S.S. A single engineered point mutation in the adenine glycosylase MutY confers bifunctional glycosylase/AP lyase activity. *Biochemistry* **39**, 10098–10109 (2000).
9. Xiang, H., Luo, L.S., Taylor, K.L. & Dunaway-Mariano, D. Interchange of catalytic activity within the 2-enoyl-coenzyme A hydratase isomerase superfamily based on a common active site template. *Biochemistry* **38**, 7638–7652 (1999).
10. Park, H.S. *et al.* Design and evolution of new catalytic activity with an existing protein scaffold. *Science* **311**, 535–538 (2006).
11. Jochens, H. *et al.* Converting an esterase into an epoxide hydrolase. *Angew. Chem. Int. Edn. Engl.* **48**, 3532–3535 (2009).
12. Chen, B. *et al.* Morphing activity between structurally similar enzymes: from heme-free bromoperoxidase to lipase. *Biochemistry* **48**, 11496–11504 (2009).
13. Raushel, F.M. Chemical biology: catalytic detoxification. *Nature* **469**, 310–311 (2011).
14. Gupta, R.D. *et al.* Directed evolution of hydrolases for prevention of G-type nerve agent intoxication. *Nat. Chem. Biol.* **7**, 120–125 (2011).
15. Tsai, P.C. *et al.* Stereoselective hydrolysis of organophosphate nerve agents by the bacterial phosphotriesterase. *Biochemistry* **49**, 7978–7987 (2010).
16. Murphy, P.M., Bolduc, J.M., Gallaher, J.L., Stoddard, B.L. & Baker, D. Alteration of enzyme specificity by computational loop remodeling and design. *Proc. Natl. Acad. Sci. USA* **106**, 9215–9220 (2009).
17. Röthlisberger, D. *et al.* Kemp elimination catalysts by computational enzyme design. *Nature* **453**, 190–195 (2008).

18. Jiang, L. *et al.* De novo computational design of retro-aldol enzymes. *Science* **319**, 1387–1391 (2008).
19. Siegel, J.B. *et al.* Computational design of an enzyme catalyst for a stereoselective bimolecular Diels-Alder reaction. *Science* **329**, 309–313 (2010).
20. Zanghellini, A. *et al.* New algorithms and an *in silico* benchmark for computational enzyme design. *Protein Sci.* **15**, 2785–2794 (2006).
21. McCall, K.A., Huang, C. & Fierke, C.A. Function and mechanism of zinc metalloenzymes. *J. Nutr.* **130**, 1437S–1446S (2000).
22. Aubert, S.D., Li, Y. & Raushel, F.M. Mechanism for the hydrolysis of organophosphates by the bacterial phosphotriesterase. *Biochemistry* **43**, 5707–5715 (2004).
23. Dyguda-Kazimierowicz, E., Sokalski, W.A. & Leszczynski, J. Gas-phase mechanisms of degradation of hazardous organophosphorus compounds: do they follow a common pattern of alkaline hydrolysis reaction as in phosphotriesterase? *J. Phys. Chem. B* **112**, 9982–9991 (2008).
24. Kuhlman, B. & Baker, D. Native protein sequences are close to optimal for their structures. *Proc. Natl. Acad. Sci. USA* **97**, 10383–10388 (2000).
25. Lawrence, M.C. & Colman, P.M. Shape complementarity at protein/protein interfaces. *J. Mol. Biol.* **234**, 946–950 (1993).
26. Davis, I.W. & Baker, D. RosettaLigand docking with full ligand and receptor flexibility. *J. Mol. Biol.* **385**, 381–392 (2009).
27. Wang, Z. & Quiocho, F.A. Complexes of adenosine deaminase with two potent inhibitors: X-ray structures in four independent molecules at pH of maximum activity. *Biochemistry* **37**, 8314–8324 (1998).
28. Pegg, S.C. *et al.* Leveraging enzyme structure-function relationships for functional inference and experimental design: the structure-function linkage database. *Biochemistry* **45**, 2545–2555 (2006).
29. Afriat, L., Roodveldt, C., Manco, G. & Tawfik, D.S. The latent promiscuity of newly identified microbial lactonases is linked to a recently diverged phosphotriesterase. *Biochemistry* **45**, 13677–13686 (2006).
30. Blum, M.M., Lohr, F., Richardt, A., Ruterjans, H. & Chen, J.C. Binding of a designed substrate analogue to diisopropyl fluorophosphatase: implications for the phosphotriesterase mechanism. *J. Am. Chem. Soc.* **128**, 12750–12757 (2006).
31. Baker, D. An exciting but challenging road ahead for computational enzyme design. *Protein Sci.* **19**, 1817–1819 (2010).
32. Kunkel, T.A. Rapid and efficient site-specific mutagenesis without phenotypic selection. *Proc. Natl. Acad. Sci. USA* **82**, 488–492 (1985).
33. Otwinowski, Z. & Minor, W. Processing of X-ray diffraction data collected in oscillation mode. *Methods Enzymol.* **276**, 307–326 (1997).
34. McCoy, A.J. *et al.* Phaser crystallographic software. *J. Appl. Crystallogr.* **40**, 658–674 (2007).
35. Winn, M.D., Murshudov, G.N. & Papiz, M.Z. Macromolecular TLS refinement in REFMAC at moderate resolutions. *Methods Enzymol.* **374**, 300–321 (2003).
36. Khersonsky, O. & Tawfik, D.S. Structure-reactivity studies of serum paraoxonase PON1 suggest that its native activity is lactonase. *Biochemistry* **44**, 6371–6382 (2005).
37. Ashani, Y. *et al.* Stereo-specific synthesis of analogs of nerve agents and their utilization for selection and characterization of paraoxonase (PON1) catalytic scavengers. *Chem. Biol. Interact.* **187**, 362–369 (2010).

Acknowledgments

We thank L. Nivon for assistance with liquid chromatography, O. Khersonsky (Weizmann Institute of Science) for providing substrates and J. Damborsky for comments on the manuscript. This work was supported by the Defense Advanced Research Projects Agency, the Defense Threat Reduction Agency and the Howard Hughes Medical Institute. P.J.G. was supported by Novo Nordisk Danmark-Amerika Fondet and Oticon Fonden.

Author contributions

S.D.K. developed the computational method for active site redesign, performed computational design and kinetic characterization of PT1–PT12, analyzed the data and wrote the paper. Y.K. designed and performed the directed evolution and library screening, wild-type activity measurements, substrate selectivity and inhibition experiments and analyzed the data and wrote the paper. P.J.G. implemented the computational redesign method, performed the computational design of PT1–PT12 and analyzed the data. R.T. determined the crystal structure of PT3.1. J.L.G. expressed and purified the designed proteins PT1–PT12. Y.S. performed pK_a calculations. Y.A., M.G., I.S., H.L. and J.L.S. synthesized nerve agents and nerve agent analogues, screened these with PT3 and determined their stereoselectivity. B.L.S. performed structural analysis and wrote the paper. D.S.T. designed the experiments and analyzed the data. D.B. designed the computational method and the experiments, analyzed the data and wrote the paper.

Competing financial interests

The authors declare no competing financial interests.

Additional information

Supplementary information is available online at http://www.nature.com/naturechemicalbiology/. Reprints and permissions information is available online at http://www.nature.com/reprints/index.html. Correspondence and requests for materials should be addressed to D.B.